2015 IEEE/RSJ International Conference on Intelligent Robots and Systems (IROS)
Congress Center Hamburg
Sept 28 - Oct 2, 2015. Hamburg, Germany

Knot-tying with Flying Machines for Aerial Construction

Federico Augugliaro, Emanuele Zarfati, Ammar Mirjan, and Raffaello D'Andrea

Abstract— **This paper addresses one of the fundamental tasks for the aerial assembly of tensile structures: aerial knot-tying. It presents a framework for representing and realizing knots with flying machines. A suitable representation of the knot topology is introduced taking into account the use of supporting elements and the characteristics of flying machines. This information is then translated into three-dimensional trajectories for the vehicle performing the aerial knot-tying task. Furthermore, preliminary results suggest that the quality of the resulting knot can be improved by the use of an iterative learning algorithm. Experiments are performed with quadrocopters to validate the proposed approach. An accompanying video shows the aerial knot-tying process.**

I. Introduction

The past years have seen an impressive increase of work on aerial manipulation: unmanned aerial vehicles are no longer passive spectators of their environment, but they physically interact with it. Force control methods for flying machines have been presented, among others, in [1]–[4], allowing them to safely be in contact with their surroundings or with humans. Researchers are also investigating how to extend the dexterity of these vehicles by equipping them with manipulators [5], [6]. These results are of particular interest for the field of robotic construction. Indeed, flying machines capable of interaction with their environment increase the potential of robotic construction: they can be used to move construction elements to locations not accessible by ground robots, to maneuver in or around existing objects to fasten construction elements, and to fly in or around already built structures to manipulate them.

As such, researchers have been motivated to study aerial construction, a field that addresses the construction of structures with the aid of flying machines [7]. During the Flight Assembled Architecture installation, a 6-m-tall tower was assembled by four quadrocopters [8], while first steps into aerial construction of truss structures have been presented in [9]. The ARCAS project [10] focuses on aerial assembly by helicopters equipped with robotic arms and an aerial 3D printer has been presented in [11].

Among the various robotic construction methods, the assembly of load-bearing structures using tensile elements, such as ropes and cables, has lately generated interest among roboticists [12]–[14] and architects [15]–[17] alike. Such elements are relatively lightweight, have a high structural strength, and can span large distances. Furthermore, they fully exploit the capabilities of flying machines and, at the same time, mitigate some of their biggest drawbacks such as limited accuracy and payload.

This paper discusses one of the fundamental tasks for the aerial assembly of tensile structures: aerial knot-tying. It defines a framework for representing and realizing knots by extending the results of [18] to account for the use of supporting elements and flying machines. Furthermore, it presents preliminary results that suggest that a learning scheme can be used to improve the final quality of the resulting knot. While rope manipulation and knot-tying have been extensively studied in the context of dexterous manipulation (see, for example, [19] and reference therein), this work approaches knot-tying by taking into account the specific characteristics of flying machines. The vehicles considered in this work are equipped with a spool and are therefore able to deploy rope as they fly. Unlike dexterous arms, flying machines do not have the ability to manipulate ropes to create arbitrary loops and crossings. They are, however, capable of freely move in space one end of the rope, giving them the ability to tie knots by flying around existing support elements and by maneuvering between already placed ropes.

The paper is organized as follows: Section II introduces a representation of knots suitable for flying machines. Section III describes how information about the knot topology is translated into three-dimensional trajectories. Section IV explores the use of an iterative learning algorithm to improve the quality of the resulting knot. Section V discusses the experimental results. A video of experiments validating the approach can be found in the accompanying multimedia submission.

II. Knot representation

Tensile structures are assembled by connecting linear elements (such as ropes) to support elements or already built structural components and are composed by concatenating two different design elements: *nodes* and *links*. A node is a point of intersection of a linear construction element with another object or with itself, whereas a rope spanned between two structural support points generates a link. In order to allow the designer of the structure to create structures with different geometries and structural properties, a library of parameterized building elements is desired. In this section, we provide a general framework that allows to describe knots (a special type of nodes) that are realizable by flying machines.

A. Knot representation

Knot theory is a branch of topology that studies mathematical knots: They differ from daily-life knots in that they

This work was supported by the Hartmann Müller-Fonds on ETH Research Grant ETH-30 12-1. F. Augugliaro, E. Zarfati, and R. D'Andrea are with the Institute for Dynamic Systems and Control, ETH Zurich, Switzerland. {faugugliaro, rdandrea}@ethz.ch. A. Mirjan is with the Chair of Architecture and Digital Fabrication, ETH Zurich, Switzerland, mirjan@arch.ethz.ch

978-1-4799-9994-1/15/$31.00 ©2015 IEEE

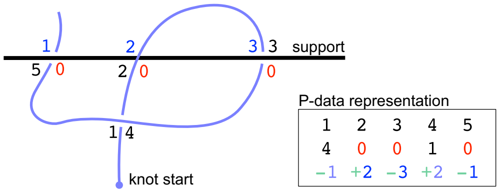

1	2	3	4	5
4	0	0	1	0
−1	+2	−3	+2	−1

Fig. 1. Projection and P-data representation of the *munter hitch* on a plane. Starting from the dot, each crossing is labeled with increasing numbers (black). Crossings with the bar are identified with a zero (red). The third row is then constructed as explained in Section II-B.

are closed because their ends are joined together. Knots are often represented using knot diagrams, where the knot is appropriately projected onto a plane and crossings are identified and numbered, thus defining the knot topology. In this work, *P-data* representation [20] is used to represent a knot in matrix form. It has been shown that multiple diagrams of the same knot exist and Reidemeister moves can be used to convert between them [21].

Knot theory alone is not enough when dealing with actual knot-tying tasks: indeed, realizable knots must be open knots, i.e. they need two free terminals (which correspond to the ends of the rope). This leads to the concept of *cross moves* [18]: A cross move adds or removes one intersection, while one terminal crosses a rope segment. This is what generates the knot with an actual rope. In [18], it has been shown that repetitions of Reidemeister moves and cross moves can be used to realize any knot-tying tasks. This is very important for the aerial knot-tying task considered in this work: As flying machines act on one end of the rope by moving it around and crossing already placed segments, their actions correspond to cross moves.

B. Introducing support elements

When building tensile structures, knots are executed to create structural elements by joining material together. Therefore, the description of a knot must include support elements, i.e. already existing elements on which the knot is actually performed. To this end, the knot representation method presented in [18] is extended to include support elements in the form of bars. Figure 1 shows the diagram of a munter hitch and its representation. Note that the fixed support is visualized in form of a horizontal line. With the projected picture, the knot representation can be constructed as follows:

1) Without loss of generality, the starting point is identified as a free terminal below the horizontal line.
2) Following the rope, each crossing is labeled with increasing numbers, resulting in the first and second row of a matrix as exemplified in Figure 1. Note that the second row contains zeros for crossings between the rope and the support element.
3) A numeric attribute is also assigned to each crossing. Its sign is negative if the rope crosses the other element underneath, it is positive otherwise; the absolute value is then assigned as follows: for rope to rope crossings, the absolute value encodes the side from which the other segment is intersected:

$$\text{from left to right} \rightarrow \{1\}; \quad \text{from right to left} \rightarrow \{2\}.$$

Rope-support crossings are numbered with increasing order from left to right.

C. Knot as a sequence of cross moves

The suggested knot representation fully defines the knot topology and includes information about the fixed support element. In order to actually tie a knot with a flying machine, a sequence of cross moves is necessary. Figure 2 shows step-by-step the cross moves that are required to create a munter hitch. It can be seen how a cross move always adds a column at the end of the P-data matrix. The sequence of cross moves required for a knot can therefore be identified from its representation. Note how the value in the second row tells *what* must be crossed (support or rope), while the third row informs about *how* (direction and orientation). A sequence of cross moves can be extracted from the P-data matrix by removing the first occurrence of any crossings that appear twice.

Note that the representation discussed in this section allows also for the description of knots that are actually not realizable with a flying machine. Indeed, depending on the knot orientation, the gravitational force will affect the shape of the rope during the realization, possibly reducing the space available to execute certain cross moves, such as passing through loops.

III. Knot Realization

The knot representation of the previous section describes the topology of knots that have been appropriately projected onto a plane, but no spatial information (such as position, orientation, or size) is contained in their representation. In this section, it is shown how a sequence of cross moves is translated into a three-dimensional trajectory for the flying machine that performs the aerial knot-tying task, thus demonstrating the appropriateness of the suggested knot representation.

A. The knot plane in three-dimensional space

The purpose of the cross moves defined above is to intersect the supporting element or an already existing segment of the rope in order to realize the desired knot. In the suggested representation, a cross move already defines whether the rope has to pass above or underneath the other element; what is missing, however, are the starting and end positions of the cross move. To this end, the following parameters are introduced to identify a plane in the three-dimensional space on which a knot is executed: the position of the knot $\vec{p}_{knot}$, the orientation of the fixed support $\vec{e}_{bar}$, and the flying machine approach direction $\vec{e}_{ad}$, which depends on the position of the previous knot and the length of the rope in-between knots. These parameters depend on the desired shape of the structure. On this plane, the following points are then identified: N, SW, and SE. Their location is motivated by the fact that the flying machine has to keep a minimum

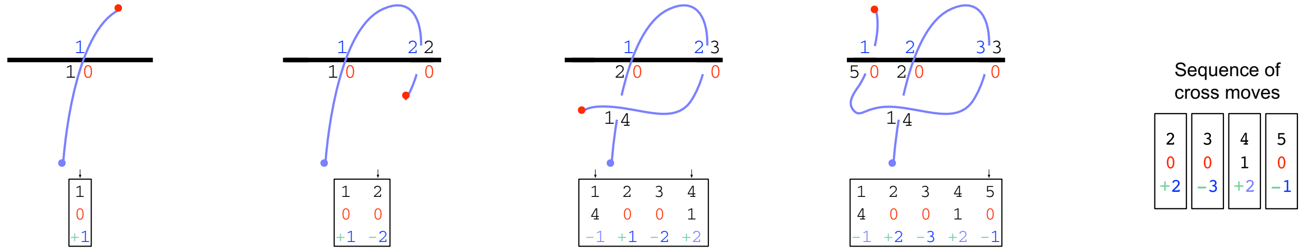

Fig. 2. A munter hitch realized with a sequence of cross moves. The red dot indicates the end of the rope attached to the flying machine. The P-data representation is shown at every step. The sequence of cross moves is extracted from the P-data matrix by removing the first occurrence of any crossings that appear twice. The cross moves are then converted into appropriate trajectories for the flying machine.

distance from both the supporting element and the already placed rope and has to pass through three different regions in order to realize the knots. These points and the associated regions can be seen in Figure 3.

After having defined the location of these points, we have to define the order in which they will be visited. The first cross move brings the vehicle coming from the approach direction to point N passing above or below the bar, according to the third row of the cross move. In the case of the munter hitch depicted in Figure 2, the second cross move leads to point SE, the third to SW, and the fourth back to N. The sequence of cross moves is translated into a sequence of positions using a predefined set of policies. A policy determines the next point to be visited based on the current point, and the current, previous, and following cross moves. It is therefore independent from the knot type.

The realization of a knot then reduces to suitable trajectories that connect points N, SW, and SE, passing either above or underneath the support element or the existing rope.

B. Cross trajectory

We define a *cross trajectory* as the spatial equivalent of a cross move in the knot representation. The initial and final points of a cross trajectory are either N, SW, or SE, and are determined by the sequence of cross moves and the set of policies, as discussed in the previous section. In this section, we define the cross trajectory to be flown by the flying machine. Because a cross move overcomes an obstacle (a rope segment or a bar), we adopt semi-circles, whose ends are denoted $\vec{p}_0$ and $\vec{p}_1$, placed on a plane orthogonal to the knot projection plane as depicted in Figure 4. Such a shape keeps the vehicle center of mass at a constant distance from the obstacle. Furthermore, we define the orientation vector $\vec{e}_\perp$, which is orthogonal to the knot plane and whose sign is given by the third value of the cross move. The position of the vehicle is then given by

$$\vec{p}(t) = r\Big(\vec{e}_\parallel \cos\left(\omega t\right) + \vec{e}_\perp \sin\left(\omega t\right)\Big), \tag{1}$$

where ω is the angular velocity, and the circle radius r and the orientation vector $\vec{e}_\parallel$ are obtained as follows:

$$r = \frac{1}{2}\|\vec{p}_0 - \vec{p}_1\|, \quad \vec{e}_\parallel = \frac{\vec{p}_0 - \vec{p}_1}{\|\vec{p}_0 - \vec{p}_1\|}. \tag{2}$$

As can be seen in Figure 4, cross trajectories are not actually performed from $\vec{p}_0$ to $\vec{p}_1$. The reason for this is that, in this work, the aerial knot-tying task is performed with quadrocopters. Continuity in the trajectory is therefore required at least up to the acceleration. Since cross trajectories are defined as constant velocity arcs, they have to be joined together appropriately, using state-to-state (position, velocity, acceleration, and heading) trajectory generation algorithms such as the one described in [22].

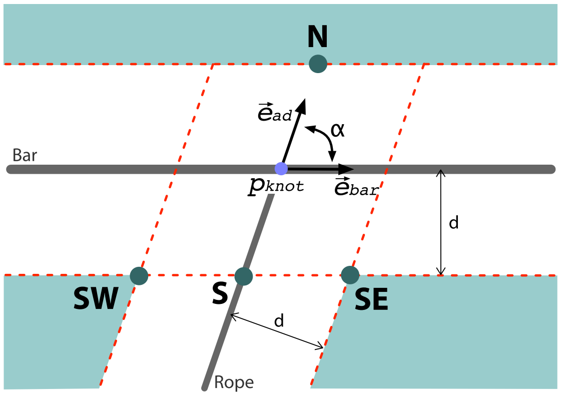

Fig. 3. The knot plane located at $\vec{p}_{knot}$ and defined by the vectors $\vec{e}_{bar}$ and $\vec{e}_{ad}$. Points N, SW, SE and S are found by imposing a minimum distance d between the flying machine tying the knot and the bar and the already placed rope. Note that at least one point in every shaded region is required in order to create the knot.

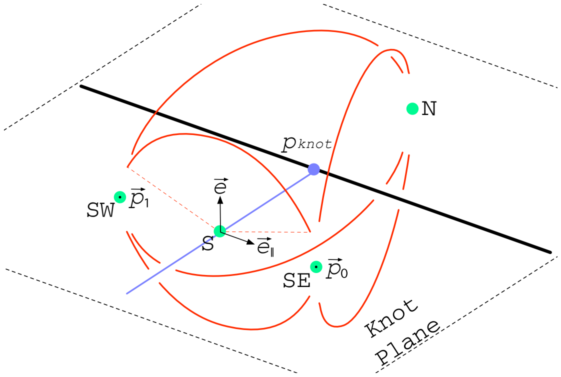

Fig. 4. Cross trajectories (red) connecting points N, SW, and SE. The black line represents the fixed support element, while the blue line indicates the approach direction.

Beside the three-dimensional coordinates, the definition of a trajectory for a quadrocopter must include the vehicle's heading. In [12], we introduced our setup, and we discussed how the vehicle's heading is fundamental for the correct deployment of the rope: since the rope release point is not located at the center of the flying machine, it should be aligned to the straight line connecting the rope release point on the vehicle to the last structural support point. Because these points are known, the cross trajectory fully defines the vehicle's heading at every time. However, since certain configurations might lead to discontinuity when the vehicle crosses the supporting element, a slew rate in the vehicle's heading is introduced.

IV. Learning realization

Experiments have shown that given the same trajectory and similar initial conditions, the final knot has very repeatable properties. However, the final result does not necessarily match the desired outcome, in that the knot is shifted along the supporting element, or that the length of the rope joining two knots is incorrect. This motivates the use of a learning algorithm to learn and compensate for these systematic errors. We use here a method based on the policy gradient learning scheme introduced in [23]: A simple model capturing the main dynamics of the system is used to derive an error correction matrix for iteratively improving the final state of the knot. This is done by measuring the final state of the knot after an iteration and then updating some key parameters of the knot-tying trajectory presented in the previous section. In this section, we present a model that captures the relevant dynamics of the knot-tying task and identify suitable trajectory parameters that strongly influence the final state of the knot.

A. Iterative learning scheme

Consider the state $q(t)$ of the rope during the knot-tying task and a model capturing its dynamics. Then, we can compute the Jacobian matrix J of the nominal final state $q(T)$ with respect to some trajectory parameters α around an initial parameter guess α_0:

$$J = \left. \frac{\partial q(T, \alpha)}{\partial \alpha} \right|_{\alpha=\alpha_0} \tag{3}$$

Assuming J is full row rank, we can then correct for the errors in the final state by modifying the chosen trajectory parameters. After iteration i, the parameters are adapted according to:

$$\alpha^{i+1} = \alpha^i - \sigma C (\Delta q)^i, \tag{4}$$

where $C = J^T(JJ^T)^{-1}$ is the (pseudo) inverse of the Jacobian matrix, σ is the step size, and $(\Delta q)^i$ is the final state error measured after iteration i. Next, we provide the rationale for the derivation of the knot model (used to calculate the matrix correction matrix C) and for the choice of the trajectory parameters α.

B. Knot model

We represent the state of a rope during the knot-tying task with $q(t) = [l(t),\, y(t)]$ and the corresponding time derivatives, where $l(t)$ is the length of the rope before the knot and $y(t)$ represents the lateral translation of a knot along the bar. This is motivated by the fact that the length of the rope between subsequent knots and the position of the knots in three-dimensional space define the shape of the structure. Because knots are performed on a fixed bar or an already placed rope, they are constrained in two dimensions, allowing thus for one translational degree of freedom only. We now need a dynamic model that captures the main behaviour of these quantities during the aerial knot-tying task.

The state of the knot is influenced by the forces acting on both ends of the knot: the force produced by the flying machine, denoted f_u, and the force due to the rope's own weight, denoted f_r. The force f_u is directly controlled through a motor mounted to the spool that releases the rope on board of the flying machine deploying the rope. Because ropes can only be subject to tension, f_u must be positive. The force f_r represents the force that acts at the other extremity of the knot. It depends on the position of the previous knot and on the current length of the rope. It can be approximated using the catenary, the curve that a rope assumes under its own weight when supported only at its ends, as follows:

$$f_r = \bar{f}_h w \cosh\left(\frac{\delta_x}{\bar{f}_h} + \operatorname{atanh}\left(\frac{\delta_z}{l}\right) - \frac{\delta_x}{2\bar{f}_h}\right), \tag{5}$$

where δ_x and δ_z are the horizontal and vertical distance between ends, w is the rope weight per meter, and $\bar{f}_h$ is the solution to:

$$\left(2\bar{f}_h \sinh\left(\frac{\delta_x}{2\bar{f}_h}\right)\right)^2 + \delta_z^2 - l^2 = 0. \tag{6}$$

Furthermore, once the rope is in contact with the bar, friction plays a significant role. When a rope is wound around a cylinder, exerting a very small force on one end of the knot enables higher loads on the other end [24]: if S_1 and S_2 are two forces acting at the two extremities of a knot, with $S_2 > S_1$, the rope will not slide if the following relationship holds:

$$S_2 < S_1 \exp\big(\mu\ |\theta|\big), \tag{7}$$

where μ represents the static friction coefficient between the rope and the cylinder, and the angle θ indicates how much the rope is wound around it. The more the rope is wound, the smaller the holding load on one side needs to be. A similar reasoning can be applied in order to capture the Coulomb friction: the more the rope is wound, the higher will be the coefficient of friction.

Friction is usually modeled as a combination of static and Coloumb friction resulting in non-smooth dynamic models. However, because we want to obtain the Jacobian matrix J, a smooth model capturing the relevant knot dynamics is required. We observe that as the rope is wound around a bar, the effects of f_u and f_r decrease as the friction force increases exponentially according to (7). Because of these considerations, we suggest the following dynamic model:

$$\ddot{q}(t) = P\frac{f_u(t) - f_r(t)}{C_1} - C_2\dot{q}(t), \tag{8}$$

where $C_i = \exp\left(\mu_i\ |\theta(t)|\right)$ capture the static and dynamic friction properties of a rope wound on a cylinder. The matrix P appropriately projects the three-dimensional forces onto the two-dimensional coordinates $l(t)$ and $y(t)$, and depends on the position $p(t)$ of the flying machine and on the direction of the bar $\vec{e}_{bar}$.

C. Parameterized knot-tying trajectory

The knot-tying trajectory described in the previous section consists of circular trajectories connecting points N, SW, and SE, and in the force profile $f_u(t)$. As expected, experiments have shown that $l(t)$ is strongly influenced by f_u. Furthermore, the lateral displacement $y(t)$ of the knot along the fixed support element is influenced by both f_u and the location of point N. These considerations lead to the following choice of trajectory parameters α for the learning algorithm: The lateral displacement of point N, denoted α_0; the value of f_u when the vehicle is on the left of the knot, denoted α_1; the value of f_u when the vehicle is on the right of the knot, denoted α_2.

The model presented in this section does not perfectly capture the complex knot-tying dynamics. Its purpose, however, is only to provide a meaningful gradient for the learning algorithm. This gradient captures not only the right direction, which has been shown in [25] to be enough for the iterative learning scheme to converge, but also the fact that as the rope is wound around the bar the knot is more and more effective. Furthermore, the resulting gradient is influenced by the knot type (i.e. the different sequence of cross moves) and the bar direction. This is important to systematically generalize the learning to different types of knots and bar configurations.

V. Experimental results

The suitability of the proposed approach to describe knots for the aerial knot-tying task is experimentally demonstrated and can be seen in the accompanying video. Furthermore, preliminary results for the iterative learning strategy are obtained by applying it to the realization of a munter hitch.

A. Experimental setup

We demonstrate the ability of quadrocopters to perform knot-tying tasks on small custom robots in the Flying Machine Arena [26], a 10m x 10m x 10m testbed for quadrocopter research. The space is equipped with a motion capture system that provides vehicle position and attitude measurements. This information is sent to a PC, which runs algorithms and control strategies, and sends commands to the quadrocopter at approximately 50Hz. The quadrocopters are equipped with a motorized rope dispenser mechanism that allows them to control the force f_u acting on the rope. The rope is not tracked.

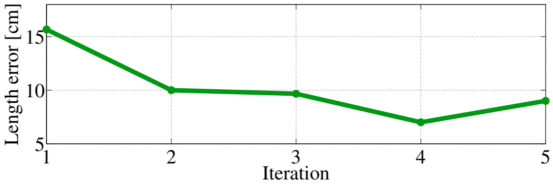

Fig. 5. The averaged length error at subsequent iterations of the learning algorithm. The error grows at iteration 5 because as the desired force f_u increases, the flight behaviour of the quadrocopter gets worse and the vehicle struggles to follow the desired trajectories. In future work, the simple model presented in this paper should be extended to capture these effects.

B. Knot realization

The accompanying video shows a quadrocopter performing the aerial knot-tying task with the framework presented in this work. For this experiment, knots were selected from a library of predefined building elements. The designer of the structure provided the following information: type and location of every knot, orientation of the fixed supports elements, and desired rope length between links. The trajectory of the flying machine was then calculated according to the methods described in sections II and III.

C. Learning the munter hitch

In this section, we provide preliminary results that validate the learning approach presented above. To this goal, we consider a munter hitch similar to the one represented in Figure 1. The knot is realized at the end of a link that connects two bars at a distance of 6.03 meters. The vectors defining the knot plane are approximated as: $\vec{e}_{bar} = [0,\ -1,\ 0]$ and $\vec{e}_{ad} = [1,\ 0,\ 0]$. The desired length of the rope joining the knots is 6.06 meters. The experiment consists of five iterations, with the knot being performed three times at every iteration i. The final state error $(\Delta q)^i$ is averaged over the three repetitions. Figure 5 shows the error for the length of the rope l. The error decreases for the first four iterations, but then starts increasing. This happens because as the desired

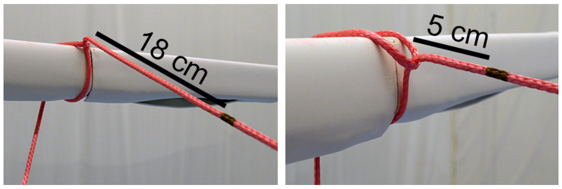

Fig. 6. The munter hitch before (left) and after (right) learning. The length error is reduced from 18 to 5 centimeters. The lateral position of the knot has also been improved.

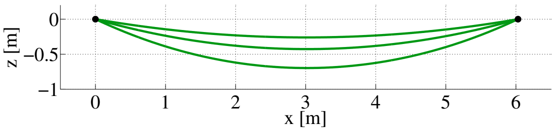

Fig. 7. The top line represents the desired rope shape. The middle shape is obtained after applying the learning scheme. The bottom shape was obtained during the first iteration. The shapes have been reconstructed using the catenary equations.

force f_u (given by the parameters α_1 and α_2) increases, the flight behaviour of the quadrocopter gets worse and the vehicle struggles to follow the desired trajectories. This is not captured in the simple model presented in the previous section: particularly, the assumption that the force f_u is constantly applied to the rope is no longer valid, as the spool mechanism is not able to compensate for the fast motions of the vehicle. However, the learning algorithm leads to noticeable improvements: The length error has been reduced (see Figure 6) and, consequently, the vertical error in the lower part of the link has decreased from 44 centimeters to 17 centimeters, as illustrated in Figure 7.

VI. Conclusion

In this paper, we presented a flexible framework that allows the representation and realization of knots for aerial knot-tying. Furthermore, preliminary results show that a learning scheme can be used to improve the final quality of the knot. These results are crucial for the assembly of complex tensile structures with flying machines and will be applied in the realization of a 1:1 footbridge construction. Future work includes the refinement of the model used for learning in order to include additional effects such as the dynamics of the flying machine deploying the rope, and the generalization of the learned parameters to other knot types and bar configurations. Furthermore, the knot representation framework can be extended to include additional supporting elements and additional cross trajectories. An interesting problem is also the realization of knots that contain loops, where the vehicle has to fly between hanging segments of the already deployed rope before tying the knot.

Acknowledgement

This work is supported by and builds upon prior contributions by numerous collaborators in the Flying Machine Arena project [27]. The authors especially thank Mark W. Mueller and Robin Ritz for the helpful discussions. The authors also thank the following people who have contributed to the hardware used in this work: Marc-André Corzillius, Mina Kamel, Gregory Baettig, Gregy Huber, Alexander Selwa, and Evan Wilson.

References

[1] L. Marconi and R. Naldi, "Control of Aerial Robots: Hybrid Force and Position Feedback for a Ducted Fan," *IEEE Control Systems*, vol. 32, no. 4, pp. 43–65, 2012.

[2] S. Bellens, J. De Schutter, and H. Bruyninckx, "A hybrid pose / wrench control framework for quadrotor helicopters," in *IEEE International Conference on Robotics and Automation*, 2012, pp. 2269–2274.

[3] F. Augugliaro and R. D'Andrea, "Admittance control for physical human-quadrocopter interaction," in *European Control Conference*, 2013, pp. 1805–1810.

[4] T. Tomic and S. Haddadin, "A unified framework for external wrench estimation, interaction control and collision reflexes for flying robots," in *IEEE/RSJ International Conference on Intelligent Robots and Systems*, 2014, pp. 4197–4204.

[5] M. Fumagalli, R. Naldi, A. Macchelli, F. Forte, A. Q. Keemink, S. Stramigioli, R. Carloni, and L. Marconi, "Developing an Aerial Manipulator Prototype: Physical Interaction with the Environment," *IEEE Robotics & Automation Magazine*, vol. 21, no. 3, pp. 41–50, 2014.

[6] F. Huber, K. Kondak, K. Krieger, D. Sommer, M. Schwarzbach, M. Laiacker, I. Kossyk, S. Parusel, S. Haddadin, and A. Albu-Schaffer, "First analysis and experiments in aerial manipulation using fully actuated redundant robot arm," in *2013 IEEE/RSJ International Conference on Intelligent Robots and Systems*, 2013, pp. 3452–3457.

[7] J. Willmann, F. Augugliaro, T. Cadalbert, R. D'Andrea, F. Gramazio, and M. Kohler, "Aerial Robotic Construction: Towards a New Field of Architectural Research," *International Journal of Architectural Computing*, vol. 10, no. 3, pp. 439–460, 2012.

[8] F. Augugliaro, S. Lupashin, M. Hamer, C. Male, M. Hehn, M. W. Mueller, J. S. Willmann, F. Gramazio, M. Kohler, and R. D'Andrea, "The Flight Assembled Architecture installation: Cooperative construction with flying machines," *IEEE Control Systems*, vol. 34, no. 4, pp. 46–64, Aug. 2014.

[9] Q. Lindsey and V. Kumar, "Distributed Construction of Truss Structures," in *Algorithmic Foundations of Robotics X*, ser. Springer Tracts in Advanced Robotics, E. Frazzoli, T. Lozano-Perez, N. Roy, and D. Rus, Eds., 2013, vol. 86, pp. 209–225.

[10] "Integrated Project Aerial Robotics Cooperative Assembly System." [Online]. Available: http://www.arcas-project.eu/

[11] G. Hunt, F. Mitzalis, T. Alhinai, P. A. Hooper, and M. Kovac, "3D printing with flying robots," in *IEEE International Conference on Robotics and Automation*, 2014, pp. 4493–4499.

[12] F. Augugliaro, A. Mirjan, F. Gramazio, M. Kohler, and R. D'Andrea, "Building tensile structures with flying machines," in *IEEE/RSJ International Conference on Intelligent Robots and Systems*, 2013, pp. 3487–3492.

[13] S. von Mammen, S. Tomforde, J. Hohner, P. Lehner, L. Forschner, A. Hiemer, M. Nicola, and P. Blickling, "OCbotics: An organic computing approach to collaborative robotic swarms," in *IEEE Symposium on Swarm Intelligence*, 2014, pp. 1–8.

[14] D. Leach, L. Wang, D. Reusser, and F. Iida, "Automatic building of a web-like structure based on thermoplastic adhesive." *Bioinspiration & biomimetics*, vol. 9, no. 3, p. 036014, Sept. 2014.

[15] A. Mirjan, F. Gramazio, and M. Kohler, "Building with Flying Robots," in *Fabricate*. gta-Verlag, 2014, pp. 266–271.

[16] "AADRL//Void - The Thread," 2015. [Online]. Available: http://vimeo.com/116910853

[17] S. Parascho, J. Knippers, D. Moritz, M. Prado, and A. Menges, "Modular Fibrous Morphologies: Computational Design, Simulation and Fabrication of Differentiated Fibre Composite Building Components," in *Advances in Architectural Geometry 2014*, P. Block, J. Knippers, N. J. Mitra, and W. Wang, Eds. Springer International Publishing, 2015, pp. 109 – 125.

[18] J. Takamatsu, T. Morita, K. Ogawara, H. Kimura, and K. Ikeuchi, "Representation for knot-tying tasks," *IEEE Transactions on Robotics*, vol. 22, no. 1, pp. 65–78, Feb. 2006.

[19] J. Schulman, J. Ho, C. Lee, and P. Abbeel, "Learning from demonstrations through the use of non-rigid registration," in *Proceedings of the 16th International Symposium on Robotics Research (ISRR)*, 2013.

[20] N. Imafuji and M. Ochiai, "Computer Aided Knot Theory Using Mathematica and Mathlink," *Journal of Knot Theory and Its Ramifications*, vol. 11, no. 06, pp. 945–954, Sept. 2002.

[21] K. Reidemeister, *Knot theory*. BCS Associates, 1983.

[22] M. W. Mueller, M. Hehn, and R. D'Andrea, "A computationally efficient algorithm for state-to-state quadrocopter trajectory generation and feasibility verification," in *IEEE/RSJ International Conference on Intelligent Robots and Systems*, 2013, pp. 3480–3486.

[23] S. Lupashin and R. D'Andrea, "Adaptive fast open-loop maneuvers for quadrocopters," *Autonomous Robots*, vol. 33, no. 1-2, pp. 89–102, Apr. 2012.

[24] W. E. Morton and J. W. Hearle, *Physical properties of textile fibres*. Textile institute, 1993.

[25] J. Z. Kolter and A. Y. Ng, "Policy search via the signed derivative," in *Robotics: science and systems*, 2009.

[26] S. Lupashin, M. Hehn, M. W. Mueller, A. P. Schoellig, M. Sherback, and R. D'Andrea, "A platform for aerial robotics research and demonstration: The Flying Machine Arena," *Mechatronics*, vol. 24, no. 1, pp. 41–54, Feb. 2014.

[27] "Flying Machine Arena." [Online]. Available: http://www.flyingmachinearena.org